2050 *Chem. Mater.* **2010,** *22,* 2050–2060
DOI:10.1021/cm903472p

CHEMISTRY OF MATERIALS
Article

Tailored Titanium Dioxide Nanomaterials: Anatase Nanoparticles and Brookite Nanorods as Highly Active Photocatalysts

Tarek A. Kandiel,[†] Armin Feldhoff,[§] Lars Robben,[‡] Ralf Dillert,[†] and Detlef W. Bahnemann*,[†]

[†]*Institut für Technische Chemie, and* [‡]*Institut für Mineralogie, Leibniz Universität Hannover, Callinstrasse 3, D-30167 Hannover, Germany, and* [§]*Institut für Physikalische Chemie und Elektrochemie, Leibniz Universität Hannover,Callinstrasse 3a, D-30167 Hannover, Germany*

Received November 14, 2009. Revised Manuscript Received January 20, 2010

High quality brookite TiO_2 nanorods have been obtained by the thermal hydrolysis of commercially available aqueous solutions of titanium bis(ammonium lactate) dihydroxide in the presence of high concentrations of urea (≥6.0 M) as an in situ OH^- source. Biphasial anatase/brookite mixtures are obtained at lower urea concentrations. The ratios between anatase and brookite can readily be tailored by the control of the urea concentration. The obtained powders have been characterized by X-ray diffraction, Raman spectroscopy, field emission-scanning electron microscopy, high-resolution transmission electron microscopy, UV−vis diffuse reflectance spectra, and nitrogen adsorption. The photocatalytic activity of pure anatase nanoparticles, of anatase/brookite mixtures, and of pure brookite nanorods has been assessed by hydrogen evolution from aqueous methanol solution as well as by the degradation of dichloroacetic acid (DCA) in aqueous solution. The results indicate that the photocatalytic hydrogen evolution activity of anatase/brookite mixtures and of pure brookite is higher than that of pure anatase nanoparticles despite of the lower surface area of the former. This behavior is explained by the fact that the conduction band edge of brookite phase TiO_2 is shifted more cathodically than that of anatase as experimentally evidenced under dark and UV−vis illumination conditions. On the contrary, in case of the photocatalytic degradation of DCA, anatase/brookite mixtures and pure brookite exhibit lower photocatalytic activity than pure anatase nanoparticles. This behavior correlates well with the surface area of the investigated powders.

Introduction

Titanium dioxide (TiO_2) is an important material for various applications such as photocatalysis, dye-sensitized solar cells, photovoltaic cells, white pigments, cosmetics, and protective coatings.[1] In nature, it exists mainly in three crystal phases: anatase (A), rutile (R), and brookite (B). Each phase displays different physical and chemical properties exhibiting different functionalities. As a bulk material, rutile is the thermodynamically stable phase; however, solution phase preparation methods for TiO_2 generally favor the anatase structure.[2] These observations are attributed to two main effects: surface energy and solution chemistry. At very small particle dimensions (nanoscale), it was reported that the transformation sequence among the three TiO_2 phases is size and pH dependent, because the energies of the three phases are sufficiently close to one another that they can be reversed by small differences in surface energy.[3] If particle sizes of the three nanocrystalline phases are equal, anatase is thermodynamically most stable at diameters less than 11 nm, brookite is most stable for crystal sizes between 11 and 35 nm, and rutile is most stable at sizes exceeding 35 nm. However, rutile is stabilized relative to anatase in very acidic solutions, whereas in very alkaline solutions anatase is stabilized relative to rutile and brookite.[4] Even the shape transformation of the TiO_2 nanocrystals was found to be controlled by the surface chemistry as confirmed by theoretical and experimental investigations.[5]

Since most of the synthetic processes produce anatase, rutile, or a mixture of them, both phases are readily employed for practical applications and extensively studied as

*To whom correspondence should be addressed. Tel.: +49-511-762-5560. Fax: +49-511-762-2774. E-mail: bahnemann@iftc.uni-hannover.de.

(1) (a) Hoffmann, M. R.; Martin, S. T.; Choi, W.; Bahnemann, D. W. *Chem. Rev.* **1995**, *95*, 69–96. (b) Chen, X.; Mao, S. S. *Chem. Rev.* **2007**, *107*, 2891–2959. (c) Fujishima, A.; Rao, T. N.; Tryk, D. A. *J. Photochem. Photobiol. C: Photochem. Rev.* **2000**, *1*, 1–21.
(2) (a) Oskam, G.; Nellore, A.; Lee, P. R.; Searson, P. C. *J. Phys. Chem. B* **2003**, *107*, 1734–1738. (b) Wang, C.; Böttcher, C.; Bahnemann, D. W.; Dohrmann, J. K. *J. Mater. Chem.* **2003**, *13*, 2322–2329.
(3) (a) Zhang, H.; Banfield, J. *J. Mater. Chem.* **1998**, *8*, 2073–2076. (b) Zhang, H.; Banfield, J. *J. Phys. Chem. B* **2000**, *104*, 3481–3487. (c) Naicker, P. K.; Cummings, P. T.; Zhang, H.; Banfield, J. f. *J. Phys. Chem. B* **2005**, *109*, 15243–15249.
(4) (a) Finnegan, M. P.; Zhang, H.; Banfield, J. F. *J. Phys. Chem. C* **2007**, *111*, 1962–1968. (b) Finnegan, M. P.; Zhang, H.; Banfield, J. F. *Chem. Mater.* **2008**, *20*, 3443–3449. (c) Mendive, C. B.; Bredow, T.; Feldhoff, A.; Blesa, M. A.; Bahnemann, D. *Phys. Chem. Chem. Phys.* **2009**, *11*, 1794–1808.
(5) (a) Barnard, A. S.; Curtiss, L. A. *Nano Lett.* **2005**, *5*, 1261–1266. (b) Saponjic, Z. V.; Dimitrijevic, N. M.; Tiede, D. M.; Goshe, A. J.; Zuo, X.; Chen, L. X.; Barnard, A. S.; Zapol, P.; Curtiss, L.; Rajh, T. *Adv. Mater.* **2005**, *17*, 965–971. (c) Feldhoff, A.; Mendive, C.; Bredow, T.; Bahnemann, D. *ChemPhysChem* **2007**, *8*, 805–809.

 Published on Web 02/10/2010

photocatalysts due to the ease of their synthesis. In contrast, the brookite phase is rarely being studied,[6] mainly due to the difficulties encountered in obtaining its pure form; however, it was reported that brookite nanocrystals have markedly high photocatalytic activities as compared to those of rutile and anatase.[7] Recently, the synthesis of pure brookite TiO_2 with different morphology such as nanorods, nanotubes, and nanoflowers has been reported,[8] but to the authors' knowledge, readily tailoring its ratio in the synthesized TiO_2 powders has not been reported up to date. Moreover, the precursors usually employed in the previously published synthetic processes are $TiCl_4$ or titanium alkoxides that are very sensitive to moisture and should, hence, be handled under inert gas and/or the processes suffer from multisteps which might lead to low yields. Thus, a great challenge remains to synthesize brookite nanorods and to tailor its ratio under simple hydrothermal conditions. Tomita et al. reported on the synthesis of nanocrystalline brookite TiO_2 employing water-soluble complexes; however, the precursor complexes were self-prepared.[9]

Here, for the first time, the synthesis of high quality brookite nanorods is reported with the advantage of tailoring the anatase/brookite ratio by a simple hydrothermal method using aqueous solutions of commercially available titanium bis(ammonium lactate) dihydroxide (TALH) in the presence of urea as an in situ OH^- source. The advantages of the use of TALH as a TiO_2 precursor are that it is a water-soluble precursor and, thus, does not require an alcohol based solution and that it is stable at ambient temperature in air, hence eliminating the need of an inert atmosphere during hydrolysis and condensation procedures.

Recently, great efforts have been made to correlate structural and physical properties with photocatalytic activities of TiO_2 powders.[10] However, the latter consisted of anatase, of anatase/rutile mixtures, and of rutile, while no attention has so far been paid to pure brookite as well as anatase/brookite mixtures. Since the photocatalytic properties of the latter have hardly been studied and little is known concerning their properties, this newly developed synthetic process provides a good opportunity to systematically investigate the relation between the physical properties and the photocatalytic activity of pure anatase, of anatase/brookite mixtures, and of pure brookite for the first time.

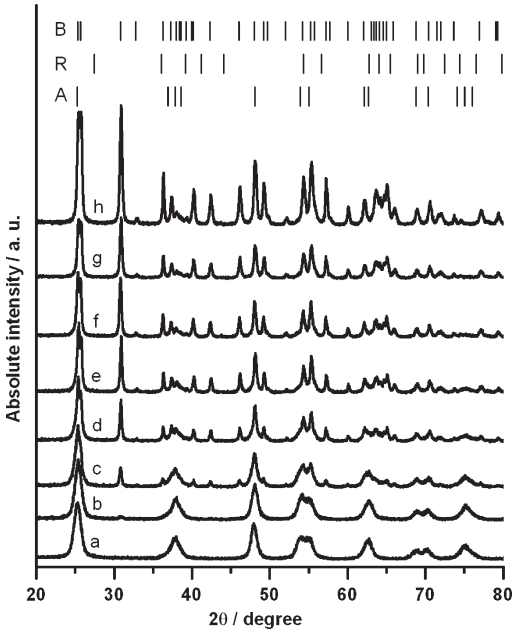

Figure 1. XRD patterns of as-synthesized nanocrystalline TiO_2 powders obtained by thermal hydrolysis of aqueous solutions of the TALH precursor at 160 °C for 24 h in the presence of different concentrations of urea: (a) 0.1 M, (b) 0.5 M, (c) 1.0 M, (d) 1.5 M, (e) 2.0 M, (f) 3.0 M, (g) 4.0 M, and (h) 6.0 M. Labels B, R, and A indicate Bragg positions for brookite, rutile, and anatase, respectively.

Results and Discussion

The thermal hydrolysis of the TALH precursor at 160 °C for 24 h in the presence of 0.1 M urea yields pure anatase nanoparticles; whereas with increasing concentration of urea up to 5.0 M, biphasial anatase/brookite mixtures are formed. At higher urea concentration (≥6.0 M), high quality brookite is obtained as proven by X-ray diffraction (XRD) measurements (Figure 1). The existence of brookite in the resultant powders is readily discernible from its (121) diffraction located at 30.81° (2θ) in the XRD pattern, where no overlapping of this peak with any peak from anatase or rutile occurs. To claim phase pure brookite, however, attention should be paid to the reflections in which overlapping with anatase reflections can occur. This is especially important for the (101) reflection of anatase and the (120) reflection of brookite. The diffraction data were analyzed by the Rietveld method considering the whole pattern and not only single peaks. Thus, a higher sensitivity for low phase contents is possible even when peak broadening due to small crystallite sizes occurs. The Rietveld analysis proves that no anatase is present in the powders synthesized via this new procedure employing 6.0 and 7.0 M urea, respectively, in the synthesis step. The small diffraction peak observed at 74.5° (2θ) (cf. Figure 1h) can readily be explained by the (104) diffraction of brookite. The quantitative phase composition and crystallite diameters of

(6) (a) Murakami, N.; Kamai, T.; Tsubota, T.; Ohno, T. *Catal. Commun.* **2009**, *10*, 963–966. (b) Addamo, M.; Bellardita, M.; Paola, A. D; Palmisano, L. *Chem. Commun.* **2006**, 4943–4945. (c) Paola, A. D; Addamo, M.; Bellardita, M.; Cazzanelli, E.; Palmisano, L. *Thin Solid Films* **2007**, *515*, 3527–3529. (d) Li, J.; Ishigaki, T.; Sun, X. *J. Phys. Chem. C* **2007**, *111*, 4969–4976. (e) Kominami, H.; Ishii, Y.; Kohno, M.; Konishi, S.; Kera, Y.; Ohtani, B. *Catal. Lett.* **2003**, *91*, 41–47.
(7) Ohtani, B.; Handa, J.; Nishimoto, S.; Kagiya, T. *Chem. Phys. Lett.* **1985**, *120*, 292–294.
(8) (a) Buonsanti, R.; Grillo, V.; Carlino, E.; Giannini, C.; Kipp, T.; Cingolani, R.; Cozzoli, P. D. *J. Am. Chem. Soc.* **2008**, *130*, 11223–11233. (b) Deng, Q.; Wei, M.; Ding, X.; Jiang, L.; Ye, B.; Wei, K. *Chem. Commun.* **2008**, 3657–3659. (c) Zhao, B.; Chen, F.; Huang, Q.; Zhang, J. *Chem. Commun.* **2009**, 5115–5117.
(9) (a) Tomita, K.; Petrykin, V.; Kobayashi, M.; Shiro, M.; Yoshimura, M.; Kakihana, M. *Angew. Chem., Int. Ed.* **2006**, *45*, 2378–2381. (b) Kobayashi, M.; Tomita, K.; Petrykin, V.; Yoshimura, M.; Kakihana, M. *J. Mater. Sci.* **2008**, *43*, 2158–2162.
(10) (a) Prieto-Mahaney, O.; Murakami, N.; Abe, R.; Ohtani, B. *Chem. Lett.* **2009**, *38*, 238–239. (b) Torimoto, T.; Nakamura, N.; Ikeda, S.; Ohtani, B. *Phys. Chem. Chem. Phys.* **2002**, *4*, 5910–5914.

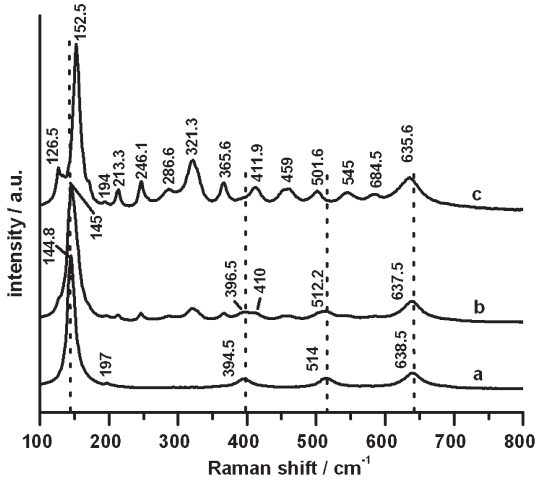

Figure 2. Raman spectra of as-synthesized nanocrystalline TiO_2 powders obtained by thermal hydrolysis of aqueous solutions of the TALH precursor at 160 °C for 24 h in the presence of different concentrations of urea: (a) 0.1 M, (b) 1.5 M, and (c) 6.0 M.

Table 1. Quantitative Phase Composition and Crystallite Diameters of Nanocrystalline TiO_2 Prepared by Thermal Hydrolysis of the TALH Precursor at 160 °C for 24 h in the Presence of Different Concentrations of Urea

urea (M)	anatase (%)	anatase crystallite size (nm)	brookite (%)	brookite crystallite size (nm)
0.1	100	11	0	
0.5	89	12	11	15
1.0	72	11	28	40
1.5	45	11	55	46
2.0	23	12	77	49
3.0	14	11	86	46
4.0	7	11	93	36
5.0	5	12	95	32
6.0	0		100	36
7.0	0		100	35

the nanocrystalline TiO_2 powders as evident from the Rietveld analysis of the XRD data are given in Table 1.

In agreement with the XRD results, the Raman spectra of the powders obtained at urea concentrations higher than 5.0 M show a rich scenario of signals, as commonly encountered for both, natural and artificial brookite (Figure 2c), whereas the powder synthesized employing 0.1 M urea exhibits the characteristic peaks of anatase (Figure 2a).[6d,8a,9b,11] The Raman spectrum of the powder synthesized employing 1.5 M urea (Figure 2b), which consists of 45% anatase and 55% brookite, indicates that there is a shift in the peaks position whenever peaks of anatase and brookite are expected to appear close to one another, as a result of the overlap between the anatase and the brookite signals, whereas the other peaks that are only related to brookite almost appear at the same position.

To obtain information about the particles morphology, some selected powders were investigated by field-emission scanning electron microscopy (FE-SEM). The micrographs of the anatase TiO_2 powder obtained by thermal hydrolysis of the TALH precursor at 160 °C for 24 h in the presence of 0.1 M urea indicate that the pure anatase powder aggregates from fine TiO_2 nanoparticles in the size range of 10 nm (as shown in Figure 3a), which is in good agreement with the particle size predicted from the XRD analysis. Figure 3b,c shows the micrographs of two different biphasial anatase/brookite mixtures, (72% anatase and 28% brookite) and (23% anatase and 77% brookite), respectively. Both micrographs indicate the formation of small nanoparticles in the size range of 10 nm and rodlike nanoparticles with diameters in the range of 25 nm. Figure 3d shows the micrograph of pure brookite obtained by the thermal hydrolysis of the TALH precursor at 160 °C for 24 h in the presence of 6.0 M urea, evincing that TiO_2 nanorods with diameters up to 25 nm and lengths up to 150 nm are formed. From XRD crystallite size data and SEM micrographs, it could be concluded that the small nanoparticles crystallize in the anatase phase while the nanorods consist of brookite; however, by definition, the crystallite size derived from the XRD analysis does not necessarily match the particle size observed by SEM. The high resolution TEM micrograph shown in Figure 4 confirms this conclusion. On the basis of spacing and angles of the lattice fringes, the rodlike particle with a diameter ca. 25 nm can be identified to be of the brookite structure.[12] The nanorod is imaged along the $[\text{-}1\text{-}2\text{-}1]_B$ zone axis, and it is faceted by $(210)_B$, 0.35 nm; $(111)_B$, 0.35 nm; and $(-110)_B$, 0.45 nm. Also, a small facet of $(012)_B$ occurs just above the tip. On the basis of the analysis of fast Fourier transforms (FFTs) of the image area, all these facets are drawn as contour lines into the experimental micrograph according to the indexing given in the inset. The longitudinal growth direction appears to be along $[001]_B$, which is the *c*-axis, and which is tilted by ca. 25° out of the image plane. Adherent to the tip of the brookite nanorod, there is a smaller particle, which is identified as anatase imaged along $[1\text{-}11]_A$. The anatase particle exhibits $(0\text{-}11)_A$ and $(10\text{-}1)_A$ planes, which share an angle of 98° and show spacings of 0.35 nm.

To understand the reaction pathway, the ratio between anatase and brookite nanoparticles has been investigated at different reaction times during the synthesis process, namely, after 3, 6, 12, 48, and 72 h, while both urea concentration (1.0 M) and temperature (160 °C) were kept constant. The Rietveld analysis of the XRD pattern of the powder obtained after a reaction time of 3 h proves the presence of anatase and brookite phases; however, the phase composition cannot be precisely determined due to the overall very low crystallinity. Whereas the Rietveld analysis of the XRD patterns of the other powders indicates that reaction times greater than 6 h have no effect on the ratio between anatase and brookite, also no change in the crystallite size was observed after a reaction time of 12 h (see Table 2).

These results are in good agreement with the previously reported fact that anatase nanoparticles with diameters $\leq$11 nm represent the most stable phase, while brookite nanoparticles with diameters between 11 and 35 nm are the most stable phase.[3] However, in the present study,

(11) Tompsett, G. A.; Bowmaker, G. A.; Cooney, R. P.; Metson, J. B.; Rodgers, K. A.; Seakins, J. M. *J. Raman Spectrosc.* **1995**, *26*, 57–62.

(12) Baur, W. H. *Acta Crystallogr.* **1961**, *4*, 214–216.

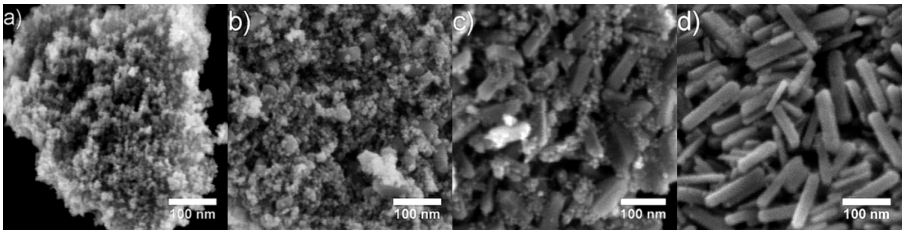

Figure 3. FE-SEM micrographs of as-synthesized nanocrystalline TiO_2 powders obtained by thermal hydrolysis of aqueous solutions of the TALH precursor at 160 °C for 24 h in the presence of different concentrations of urea: (a) 0.1 M, (b) 1.0 M, (c) 2.0 M, and (d) 6.0 M.

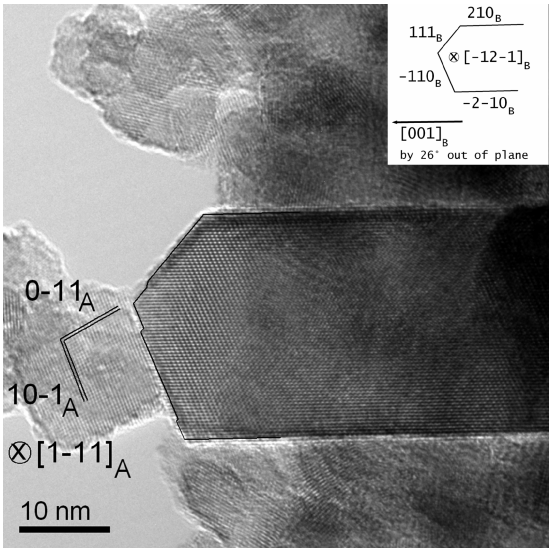

Figure 4. High-resolution transmission electron micrograph of as-synthesized nanocrystalline TiO_2 powder obtained by thermal hydrolysis of aqueous solutions of the TALH precursor at 160 °C for 24 h in the presence of 1.0 M urea. The rodlike particle of ca. 25 nm in diameter is brookite imaged along the $[-12-1]_B$ zone axis (see inset). The smaller particle of ca. 15 nm in size is anatase imaged along $[1-11]_A$. The labels A and B refer to anatase and brookite, respectively.

Table 2. Quantitative Phase Composition and Crystallite Diameters of Nanocrystalline TiO_2 Prepared by Thermal Hydrolysis of the TALH Precursor at Different Reaction Times and Temperatures in the Presence of 1.0 M of Urea

T (°C)	reaction time (h)	anatase (%)	anatase crystallite size (nm)	brookite (%)	brookite crystallite size (nm)
160	6	77	6	23	20
160	12	77	10	23	38
160	24	72	12	28	40
160	48	72	11	28	40
160	72	75	14	25	40
120	24	82	6	18	22
200	24	87	13	13	32

brookite has nanorod morphology with diameters up to 25 nm and lengths up to 150 nm. These results also indicate that there is no phase transformation between anatase and brookite under the applied conditions and that there is no further particle growth with an increase of the reaction time as proven by the scanning electron microscopy. Depending on these results, more likely, brookite does not form through intermediate phases, rather the brookite seeds are directly formed from the TALH complex and continue to grow in the solution until reaching the appropriate size in good agreement with a previously reported observation.[9b] The effect of temperature on the anatase/brookite ratio has also been investigated at 120 and 200 °C. The Rietveld analysis of the XRD patterns of the obtained powders indicates that the temperature has a minor effect on the anatase/brookite ratio (see Table 2). It was also noted that the final pH in all experimental runs is about 9.9 when urea concentrations higher than 0.5 M were employed during the synthesis process. This reveals that under the present conditions the increase of the brookite content in the obtained powders at different urea concentrations is not governed by the final pH but rather by the dosing of the in situ produced OH^-. To ensure the importance of the in situ OH^- generation for the formation of the brookite phase, one experiment has been performed at pH 9.9 employing ammonium hydroxide instead of urea for 24 h at 160 °C. The Rietveld analysis of the XRD pattern of the isolated powder indicates that the product is 100% anatase. At higher ammonium hydroxide concentrations (up to 8.0 M), anatase/brookite mixtures have indeed been obtained. However, even at 8.0 M NH_4OH, the ratio of the brookite phase in the isolated powders does not exceed 20% according to the Rietveld analysis of the respective XRD patterns.

From the results reported so far, it becomes obvious that the anatase/brookite ratio is mainly controlled by the concentration of urea. Urea hydrolyzes extremely slowly at room temperature but more rapidly at temperatures higher than 90 °C producing OH^- ions.[13] At low urea concentrations, the in situ produced OH^- ion dosing is only sufficient for a slow hydrolysis of the TALH precursor leading to the formation of pure anatase nanoparticles. An increase in the urea concentration leads to an increase in the OH^- ion dosing resulting in rapid thermal hydrolysis of the TALH precursor and the formation of both anatase and brookite seeds. From the experimental results presented here, it can be concluded that the increase of the in situ OH^- ion dosing favors the formation of brookite. Once the formation of brookite or anatase seeds has occurred, it seems reasonable that the growth of the crystallites requires lower activation energy than the transformation to another phase. The increase of the urea concentration, also, might somehow effect the stereo conformation of the TALH complex so that the complex structure resembles the architecture of brookite. This will facilitate the brookite formation as previously

(13) (a) Hanprasopwattana, A.; Rieker, T.; Sault, A. G.; Datye, A. K. *Catal. Lett.* **1997**, *45*, 165–175. (b) Liu, L.; Zhao, Y.; Liu, H., 2; Kou, H.; Wang, Y. *Nanotechnology* **2006**, *17*, 5046–5050.

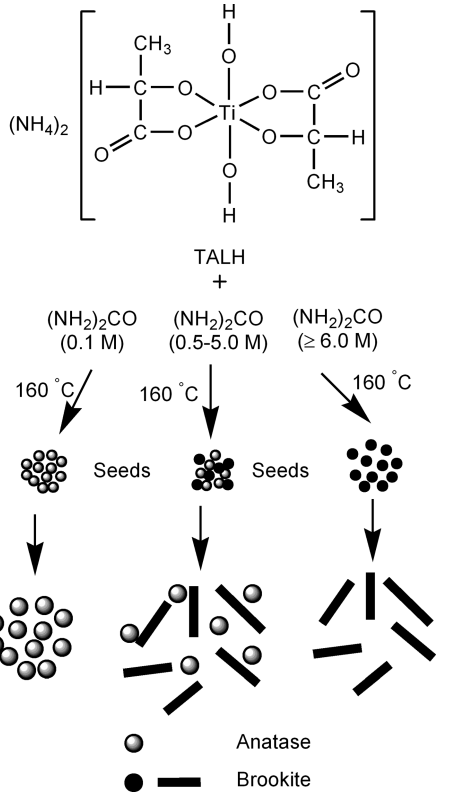

Figure 5. Proposed routes for the formation of anatase nanoparticles and brookite nanorods.

suggested;[9a] however, a complexation of urea with Ti(IV) appears to be unlikely, since urea complexes with Ti(IV) should have a rather low stability as compared with, e.g., lactate. If urea reacts with Ti(IV) as bidentate ligand, it will form a four-membered ring that is less stable than a five-membered ring formed by lactate. Even the possibility of urea reacting as monodentate ligand can be readily excluded by the fact that no change in the UV−vis spectra of the TALH complex was observed after treatment with urea indicating that there is no ligand exchange. On the basis of the experimental results, the proposed reaction pathways are summarized in Figure 5.

The photocatalytic activity of the tailored anatase/brookite mixtures has been assessed by determining the photonic efficiencies of the molecular hydrogen production from aqueous methanol solutions and of the degradation of dichloroacetic acid (DCA) in aqueous solution, respectively. Before the photocatalytic hydrogen evolution tests, the TiO_2 powders have been loaded with 0.5 wt % Pt nanoparticles using colloidal Pt solution. Colloidal Pt solution has been used to avoid the probability of the change of the particle size of the Pt nanoparticles during the Pt loading to ensure that the difference in the photocatalytic activity can clearly be attributed to the properties of the tested TiO_2 powders. When TiO_2 absorbs a photon, the energy of which exceeds its bandgap energy, an electron (e^-)/hole (h^+) pair is generated. Both e^- and h^+ can either migrate to the TiO_2 surface and react with adsorbed reactants in a photocatalytic process or may undergo an undesired recombination. In the presence of an electron donor, such as methanol, and in the absence of

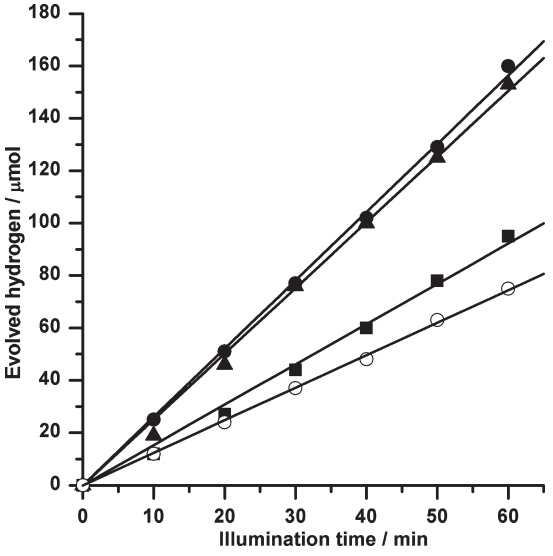

Figure 6. Time course of H_2 evolution over Pt loaded (■) anatase nanoparticles, (●) anatase/brookite mixture (28% brookite and 72% anatase), (▲) brookite nanorods, and (○) Degussa P25; 0.5 g L^{-1} catalyst, 75 mL of aqueous methanol solution (4.93 mol L^{-1}), 0.5 wt % Pt, and UG1 Black filter.

O_2, the excess holes will be consumed and the photogenerated electrons will be trapped near the surface forming trivalent titanium (Ti^{3+}) instead of reducing H^+. This phenomenon has been observed by Bahnemann et al.[14] in laser-flash photolysis experiments employing suspensions of colloidal TiO_2. Loading the TiO_2 surface with small Pt islands creates sinks for the electrons, thus facilitating the separation of e^-/h^+ pairs photogenerated in TiO_2 and promoting the formation of H_2 gas.[15]

The photonic efficiencies (ξ) of hydrogen production have been calculated by dividing the rate of hydrogen evolution by the photon flux ($\xi = R/I_0$).[16] The rate of hydrogen evolution has been calculated from the slope of the time course of the hydrogen production upon UV−vis illumination (as an example, see Figure 6). The photon flux has been calculated by employing ferrioxalate actinometry[17] performed under the same conditions as the rate of hydrogen evolution measurements to eliminate any errors associated with the influence of light reflections and reactor geometry. At this point, it is also important to emphasize that the experimental conditions have been designed to ensure that the incident light is completely absorbed by the photocatalysts (except for the fraction of the light that is backscattered). Depending on the diffuse reflectance spectra of the investigated powders (see for example Figure 10), it is reasonable to assume that the fraction of the backscattered light is almost identical

(14) Bahnemann, D.; Henglein, A.; Lilie, J.; Spanhel, L. *J. Phys. Chem.* **1984**, *88*, 709–711.
(15) (a) Bahnemann, D.; Henglein, A.; Spanhel, L. *Faraday Discuss. Chem. Soc.* **1984**, *78*, 151–163. (b) Wang, C.; Pagel, R.; Bahnemann, D. W.; Dohrmann, J. K. *J. Phys. Chem. B* **2004**, *108*, 14082–14092. (c) Kiwi, J.; Grätzel, M. *J. Phys. Chem.* **1984**, *88*, 1302–1307.
(16) (a) Serpone, N.; Terzian, R.; Lawless, D.; Kennepohl, P.; Sauve, G. *J. Photochem. Photobiol. A: Chem.* **1993**, *73*, 11–16. (b) Serpone, N.; Salinaro, A. *Pure Appl. Chem.* **1999**, *71*, 303–320.
(17) (a) Hatchard, C. G.; Parker, C. A. *Proc. R. Soc. Ser. A* **1956**, *235*, 518–536. (b) Kirk, A. D.; Namasivayam, C. *Anal. Chem.* **1983**, *55*, 2428–2429.

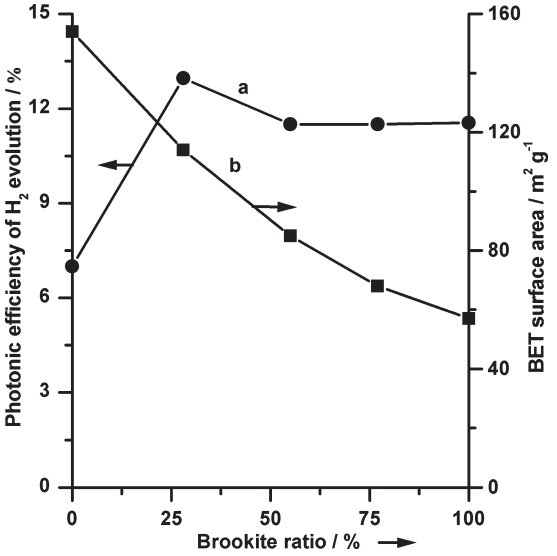

Figure 7. Relation between the photonic efficiency, the surface area and the content of brookite: (●, a) photonic efficiency and (■, b) surface area. Conditions in case of photonic efficiency measurements: 0.5 g L^{-1} catalyst, 75 mL of aqueous methanol solution (4.93 mol L^{-1}), 0.5 wt % Pt, and UG1 Black filter.

for all catalysts synthesized here. Thus, the photonic efficiencies have been calculated assuming that all photocatalysts absorb the same amount of the light. Figure 7a shows that the photonic efficiency of the photocatalytic hydrogen production increases as the content of the brookite phase in the investigated powders increases, followed by a slight decrease and subsequently a leveling off. The relation between the photonic efficiency and the BET surface area has also been investigated (Figure 7b). Surprisingly, as shown in Figure 7a,b, there is a reverse dependency between the photonic efficiencies of photocatalytic hydrogen production and the BET surface areas of the investigated powders relative to the brookite content. As the brookite content increases in the investigated powders, the photonic efficiency increases despite the simultaneous decrease of the surface area. Thus, the increase in the photonic efficiency cannot be explained by a dependence on the surface area. Recently, Prieto-Mahaney et al.[10a] reported correlations between structural and physical properties and photocatalytic activities of H_2 evolution from aqueous methanol solution over 35 TiO_2 powders exclusively consisting of anatase, of anatase/rutile mixtures, and of rutile. They found, after statistical multivariable analyses, a negative correlation coefficient between the photocatalytic activity of H_2 evolution and the BET surface area. On the contrary, large positive correlation coefficients between the photocatalytic activity of H_2 evolution and the secondary particle size (SPS) as well as the primary particle size (PPS) were observed. Accordingly, these authors concluded that large secondary particles composed of large primary particles with fewer crystalline defects are preferable. Here, for the investigated TiO_2 powders, there is no apparent change in the primary particle size (PPS) for anatase nanoparticles and for brookite nanorods as concluded from the measured crystallite sizes (see Table 1), but the secondary particle size (SPS), which is defined as a volume-average particle size, is expected to change with an increase of the brookite content, i.e., the volume-average particle size of anatase/brookite mixtures and of brookite nanorods is expected to be larger than that of anatase nanoparticles due to the fact that brookite nanorods exhibit a larger particle size than anatase nanoparticles (see FE-SEM and TEM micrographs, Figures 3a,b, c,d and 4, respectively). Thus, it becomes obvious that the increased photocatalytic activity of anatase/brookite mixtures and of pure brookite nanorods relative to that of anatase nanoparticles can be explained neither by surface area nor by the primary particle size. The expected larger secondary particle size of anatase/brookite mixtures and of pure brookite nanorods relative to that of anatase nanoparticles might be one reason for their high photocatalytic activity; however, it seems more reasonable that the large crystallite size of brookite nanorods in comparison with that of anatase nanoparticles should be regarded as another reason. The large crystallite size might lead to a low density of crystalline defects; hence, it will increase the photocatalytic activity of H_2 evolution from aqueous methanol solution.[18] In fact, the dependence of the photocatalytic activity on the physical properties is indeed very complex.[10a] An examination of the flatband potential of the different TiO_2 phases might also be helpful to understand this behavior. In general, the potential of the valence band of titanium dioxide ($\sim$+ 3.0 V vs NHE) is considerably more positive than the potential required for methanol oxidation (+1.24 V vs NHE).[15b] In contrast, the potential of the conduction band electrons in the anatase phase is only positioned cathodically by approximately 200 mV more negatively than the potential required for the hydrogen evolution, whereas, in case of rutile, it almost coincides with the potential required for the hydrogen evolution.[19] Any further cathodic shift of the flatband potential of TiO_2 will, therefore, favor reduction reactions initiated by the conduction band electrons such as the photocatalytic hydrogen production. Thus, the increased photocatalytic activity observed upon the increase of the brookite content might be resulting from a cathodic shift of the flatband potential of the brookite phase as compared with that of the anatase phase. To investigate this assumption experimentally, the flatband potential of both the anatase nanoparticles and the brookite nanorods, has been measured. The flatband potentials of semiconductor electrodes at the semiconductor/electrolyte junction can be obtained from Mott−Schottky plots (measured in the dark) using the following eq 1:[20]

$$\frac{1}{C^2} = \frac{2}{\varepsilon_{TiO_2}\varepsilon_0 e_0 N_D}\left(E - E_{FB} - \frac{kT}{e_0}\right) \qquad (1)$$

(18) Amano, F.; Prieto-Mahaney, O.; Terada, Y.; Yasumoto, T.; Shibayama, T.; Ohtani, B. *Chem. Mater.* **2009**, *21*, 2601–2603.
(19) (a) Karakitsou, K. E.; Verykios, X. E. *J. Phys. Chem.* **1993**, *97*, 1184–189. (b) Rao, M. V.; Rajeshwar, K.; Pal Verneker, V. R.; DuBow, J. *J. Phys. Chem.* **1980**, *84*, 1987–1991.
(20) Baumanis, C.; Bahnemann, D. W. *J. Phys. Chem. C* **2008**, *112*, 19097–19101.

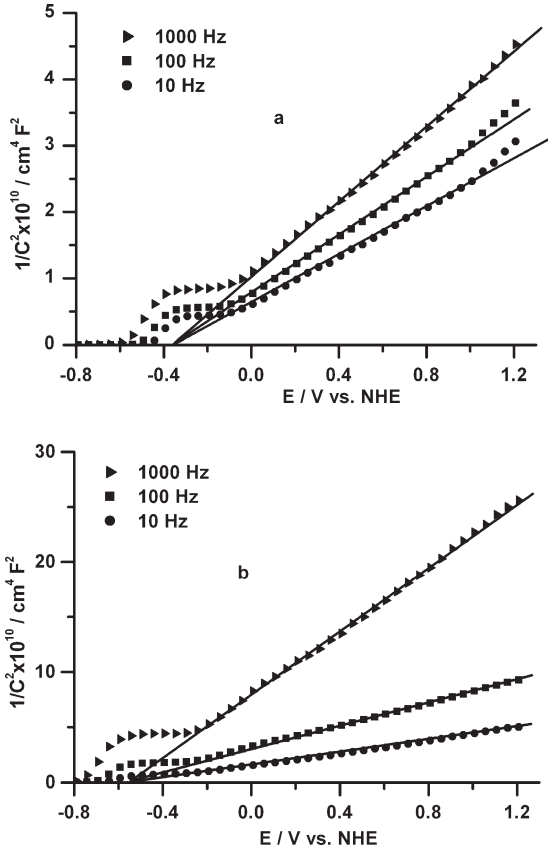

Figure 8. Mott−Schottky plots obtained at different frequencies for the TiO_2 films electrodes prepared with (a) anatase nanoparticles and (b) brookite nanorods. TiO_2 film/Ag/AgCl/Pt in 0.1 M KCl, pH 7.0.

with ε_0 being the permittivity of free space, ε_{TiO_2} the permittivity of the semiconductor electrode, e_0 the elementary charge, N_D the donor density, E the applied potential, E_{FB} the flatband potential, k the Boltzmann constant, T the temperature of operation, and C the space charge capacitance.

Plotting $(1/C^2)$ vs E should, thus, yield a straight line, intersecting the potential axis at E_{FB}. The Mott−Schottky plots obtained for the anatase nanoparticles and the brookite nanorods prepared here are shown in Figure 8a, b, respectively. The results indicate that the flatband potential of the anatase nanoparticles is $E_{FB} = -0.35$ V vs NHE, whereas the flatband potential of the brookite nanorods taken from Figure 8b is $E_{FB} = -0.54$ V vs NHE. To ensure that the potential of e_{CB}^- in the brookite nanorods is shifted cathodically in comparison with that of the anatase nanoparticles, the quasi-Fermi levels ($^*E_f$) of anatase nanoparticles and brookite nanorods have, furthermore, been determined under UV illumination according to the method of Roy et al.[21] Employing this method, the photovoltage of a powder suspension is measured in the presence of a pH-independent redox couple such as methylviologen dichloride (MV^{2+}, $E_{red} = -0.445$ V vs NHE) as a function of the pH value.

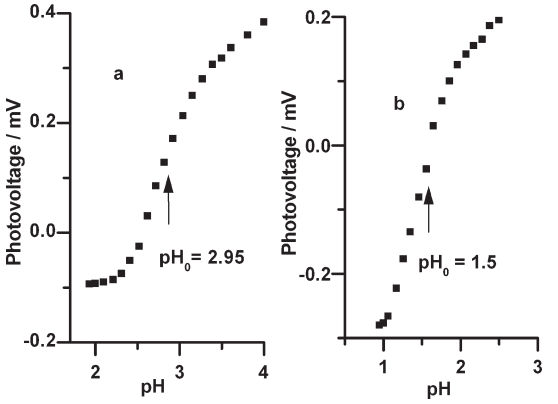

Figure 9. Photovoltage vs suspension pH value measured for (a) anatase nanoparticles and (b) brookite nanorods in 0.1 M KNO_3 in the presence of MV^{2+}.

The $^*E_f$ of the anatase nanoparticles and the brookite nanorods have been obtained from the inflection points (pH_0) of the photovoltage−pH curves (cf. Figure 9a,b). The obtained pH_0 values can readily be converted to the quasi-Fermi potentials at pH 7 by equation

$$^*E_F(\text{pH } 7) = E_{red} + 0.059\,(pH_0 - 7) \qquad (2)$$

From the results shown in Figure 9 the quasi-Fermi level of the anatase nanoparticles is calculated to be $^*E_f = -0.68$ V vs NHE, whereas the quasi-Fermi level of the brookite nanorods is found to be $^*E_f = -0.77$ V vs NHE. The quasi-Fermi level is found to be more negative than the flatband potential by 0.33 and 0.23 V for anatase nanoparticles and brookite nanorods, respectively. These differences can be explained by the fact that the former was measured under illumination in an aqueous TiO_2 suspension while the latter was measured in the dark employing TiO_2 films. Regardless of this shift, clearly, the results of both independent methods performed under dark and illuminated conditions, respectively, indicate that both the flatband potential and the quasi-Fermi level of brookite nanorods are positioned more cathodically as compared with the respective values of anatase nanoparticles (cf. Table 3 second and third columns). Even for the anatase/brookite mixture, the flatband potential and the quasi-Fermi level was found to be more negative than that of the pure anatase nanoparticles (cf. Table 3 second and third columns). Assuming that the flatband potential and the quasi-Fermi level are a direct measure of the lower edge of the conduction band, the value of the latter was calculated as the mean value of the former (cf. Table 3 fourth column). It can, hence, be concluded that the conduction band of brookite TiO_2 is positioned by about 140 mV more cathodically than that of the anatase phase (cf. Table 3, last column). As the valence band position of TiO_2 appears to be rather insensitive to the lattice structure,[22] this cathodic shift should reflect an effective increase of the bandgap energy of the brookite phase by 140 mV as compared with that of the anatase phase. To

(21) (a) Roy, A. M.; De, G. C.; Sasmal, N.; Bhattacharyya, S. S. *Int. J. Hydrogen Energy* **1995**, *20*, 627–630. (b) Long, M.; Cai, W.; Kisch, H. *J. Phys. Chem. C* **2008**, *112*, 548–554. (c) Gärtner, M.; Dremov, V.; Müller, P.; Kisch, H. *ChemPhysChem* **2005**, *6*, 714–718.

(22) Zhang, H.; Chen, G.; Bahnemann, D. W. *J. Mater. Chem.* **2009**, *19*, 5089–5121.

Table 3. Flatband Potentials (E_{FB}), Quasi-Fermi Levels ($^*E_f$), and Conduction Band Potentials (E_{CB}) of Anatase Nanoparticles, Anatase/Brookite Mixture (72% Anatase and 28% Brookite), and Brookite Nanorods

nanomaterials	E_{FB} [V vs NHE]	$^*E_f$ [V vs NHE]	E_{CB} (calc) [V vs NHE]
anatase nanoparticles	−0.35	−0.68	−0.51
anatase/brookite mixture	−0.41	−0.71	−0.56
brookite nanorods	−0.54	−0.77	−0.65

experimentally prove this assumption, the bandgap energies of both materials have been determined by plotting the modified Kubelka−Munk function $[F(R)E]^{1/2}$ calculated from the optical absorption spectrum vs the energy of the exciting light E assuming that TiO_2 has an indirect optical transition (Figure 10).[23] The intercepts of the straight lines a and b plotted in Figure 11 yield bandgap energies of 3.18 and 3.31 for the anatase nanoparticles and the brookite nanorods, respectively. The difference in bandgap energies of the two nanomaterials of 130 mV coincides extremely well with the cathodic shift of the potential of the e_{CB}^- in the brookite nanorods determined by two completely independent experimental methods. Thus, in the case of the brookite nanorods, the driving force for the proton reduction is higher than that in the case of the anatase nanoparticles. This might also explain why anatase/brookite mixtures and pure brookite nanorods exhibit higher photocatalytic activity than anatase nanoparticles despite their decreasing surface area. The conduction band of brookite TiO_2 is positioned about 140 mV more cathodically than that of anatase. This should facilitate interfacial electron transfer while the resulting energy barrier would suppress back electron transfer. Consequently, the holes left in the valence band of brookite efficiently oxidize organic substrates, while the electrons that have been transferred into the anatase phase are consumed by the reduction of H^+ at the Pt nanoparticles. This will lead to a better charge carrier separation and, hence, to an increase of the photocatalytic activity similar to that usually assumed for anatase/rutile mixtures.[24] The photonic efficiencies of photocatalytic H_2 evolution have been compared with those of TiO_2 Degussa P25 under the same conditions. The results reveal that the newly synthesized TiO_2 photocatalysts (anatase/brookite mixtures and pure brookite) exhibit considerable higher activity than TiO_2 Degussa P25. For example, the TiO_2 photocatalyst (72% anatase and 28% brookite) has a photonic efficiency twice as high than that of TiO_2 Degussa P25 (see Figure 6).

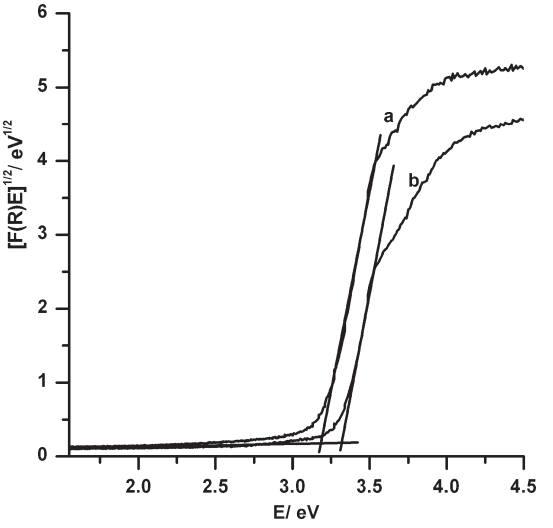

Figure 10. Plot of the modified Kubelka−Munk function versus the energy of light absorbed for (a) anatase nanoparticles and (b) brookite nanorods.

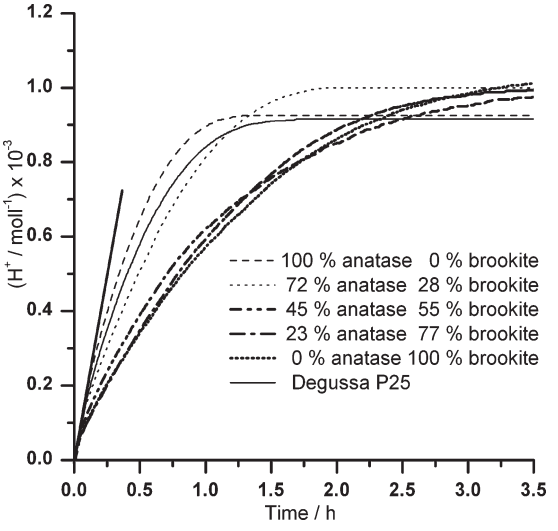

Figure 11. Time course of DCA photocatalytic degradation using anatase nanoparticles, anatase/brookite mixtures, brookite nanorods, and Degussa P25 as a photocatalysts.

The photocatalytic degradation of dichloroacetic acid, DCA, as model pollutant was performed at pH 3 using a pH-stat technique as described by Bahnemann et al.[25] (see Experimental Section). Figure 11 shows the time profiles of the DCA degradation on the investigated TiO_2 powders. The photonic efficiencies (ζ) of the photocatalytic degradation of DCA were calculated as the ratio of the initial degradation rate of DCA and the incident photon flux. The relation between the brookite/anatase ratios and the photonic efficiencies as well as the surface areas of the investigated powders was investigated (cf. Figure 12). As shown in Figure 12a, the photonic efficiency of the DCA degradation decreases as the brookite content increases in the investigated powders, on the contrary to the behavior observed for the photocatalytic hydrogen evolution from aqueous methanol solutions. Apparently,

(23) (a) Tauc, J.; Grigorovici, R.; Vanuc, A. *Phys. Status Solidi* **1966**, *15*, 627. (b) Sakthivel, S.; Janczarek, M.; Kisch, H. *J. Phys. Chem. B* **2004**, *108*, 19384–19387.

(24) (a) Zachariah, A.; Baiju, K. A.; Shukla, S.; Deepa, K. S.; James, J.; Warrier, K. G. K. *J. Phys. Chem. C* **2008**, *112*, 11345–11356. (b) Li, G.; Ciston, S.; Saponjic, Z. V.; Chena, L.; Dimitrijevic, N. M.; Rajh, T.; Graya, K. A. *J. Catal.* **2008**, *253*, 105–110. (c) Miyagi, T.; Kamei, M.; Mitsuhashi, T.; Ishigaki, T.; Yamazaki, A. *Chem. Phys. Lett.* **2004**, *390*, 399–402. (d) Liu, Z.; Zhang, X.; Nishimoto, S.; Jin, M.; Tryk, D. A.; Murakami, T.; Fujishima, A. *Langmuir* **2007**, *23*, 10916–10919.

(25) (a) Bahnemann, D. W.; Bockelmann, D.; Goslich, R.; Hilgendorff, M.; Weichgrebe, D. Photocatalytic detoxification: novel catalysts, mechanisms and solar applications. In *Trace Metals in the Environment 3: Photocatalytic Purification and Treatment of Water and Air*; Ollis, D. F.; Al-Ekabi, H., Eds.; Elsevier Science: Amsterdam, The Netherlands, 1993; pp 301−319. (b) Menéndez-Flores, V. M.; Friedmann, D.; Bahnemann, D. W. *Int. J. Photoenergy* **2008**, *ID*, 280513.

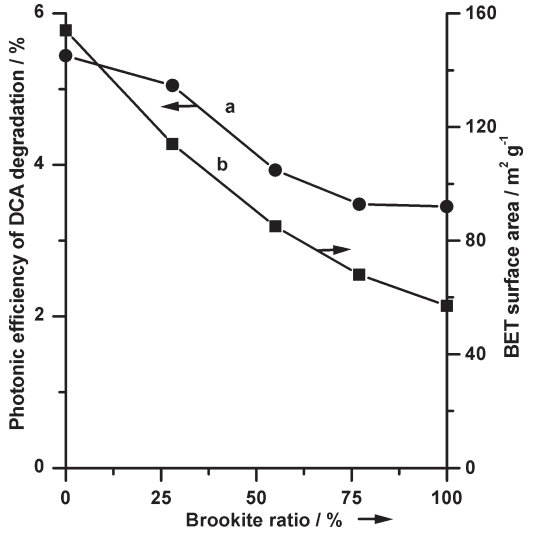

Figure 12. Relation between the photonic efficiency, the surface area, and the content of brookite: (●, a) photonic efficiency and (■, b) surface area. Conditions in case of photonic efficiency measurements: 0.5 g L^{-1} catalyst, 60 mL of aqueous 1 mmol L^{-1} DCA, and pH 3.

the dependency of the photonic efficiency of the DCA degradation and of the surface area upon the content of brookite in the investigated powders exhibit the same trend (Figure 12a,b). With increasing brookite content in the investigated powders, both the photonic efficiency and the surface area decrease. Thus, the decrease of the photocatalytic activity in this case can be attributed to the decrease of the surface area. It is often assumed that the larger the specific area, and thus the higher the adsorption of the organic molecules, the higher will be the photocatalytic degradation rate. However, the observed differences in photocatalytic activity, in general, cannot be interpreted using only a single property of the photocatalysts.[26] The photonic efficiencies of DCA degradation have been compared with those of TiO_2 Degussa P25. The results revealed that anatase nanoparticles exhibit higher photonic efficiency than TiO_2 Degussa P25 whereas anatase/brookite mixtures and pure brookite have lower photonic efficiencies than TiO_2 Degussa P25 (see Figure 11).

Conclusions

In conclusion, high quality brookite nanorods have been obtained by thermal hydrolysis of aqueous solutions of titanium bis(ammonium lactate) dihydroxide (TALH) in the presence of high concentrations of urea ($\geq$6.0 M) as an in situ OH^- source. Biphasial anatase/brookite powders are obtained at lower urea concentrations. The ratio between anatase and brookite can readily be tailored by controlling the urea concentration. The photocatalytic activity of pure anatase, of anatase/brookite mixtures, and of pure brookite nanorods has been assessed by the hydrogen evolution from aqueous methanol solutions and by the degradation of dichloroacetic acid (DCA) in aqueous solution. The results indicate that the photocatalytic hydrogen evolution activity of anatase/brookite mixtures and of pure brookite suspensions is higher than that of pure anatase despite the fact that the former exhibits a lower surface area. This behavior can be explained by the fact that the flatband potential of the brookite nanorods is shifted by 140 mV more cathodically than the flatband potential of the anatase nanoparticles. However, in the case of the photocatalytic degradation of DCA, anatase/brookite mixtures and pure brookite suspensions are photocatalytically less active than anatase nanoparticles alone. This behavior is readily explained by the higher surface area of the latter.

Experimental Section

Hydrothermal Synthesis. Thermal hydrolysis experiments were carried out in a 250 mL Teflon cup enclosed in a stainless steel autoclave (Berghof, DAB-3). Ten milliliters of TALH aqueous precursor (50%, Sigma-Aldrich) and the prepared aqueous solution containing the desired amount of urea (Sigma-Aldrich) were mixed followed by the addition of deionized water to reach a final volume of 100 mL. The resulting solution was transferred into the Teflon cup. Afterward, the Teflon cup was sealed in the autoclave and placed into an electric furnace held at 160 °C for a required time. Then, the autoclave was cooled in air. The resulting powders were separated by centrifugation, washed with water three times, and dried overnight at 60 °C in an oven. The yield is found to be not less than 97% of the expected yield from the complete thermal hydrolysis of the available TALH complex.

Preparation of Pt loaded TiO_2. Colloidal Pt (particle diameters ca. 3 nm) has been prepared by reduction of H_2PtCl_6 with sodium citrate.[14] Excess ions in the resulting colloidal suspension were removed with an ionexchange resin (Amberlite MBl) until a specific conductivity of ca. 3 μS cm^{-1} was reached. Pt-loaded TiO_2 was prepared by suspending 0.25 g of TiO_2 powder in 80 mL of deionized water by sonication, followed by the addition of the desired amount of as-prepared colloidal Pt under continuous magnetic stirring. The stirring was kept overnight to ensure the homogeneous dispersion of the Pt nanoparticles. After evaporation under vacuum at room temperature, a grayish powder was obtained. The obtained powder was dried at 60 °C in an oven overnight.

Characterization. XRD data for the Rietveld phase analysis of TiO_2 have been recorded on a Phillips PW1800 diffractometer using a reflection geometry with variable divergence slits, Cu $K\alpha_{1,2}$ radiation, and a secondary monochromator. Three thousand data points were collected with a step width of 0.02° and 2 s measurement time per step in the 2θ range from 20 to 80°. The phase analysis by the Rietveld method was carried out using the TOPAS 2.0 (Bruker AXS) software. During the refinements, general parameters such as scale factors, one background parameter, and the zero point error were optimized. Profile shape calculations were carried out on the basis of standard instrumental parameters using the fundamental parameter approach implemented in the program, varying also the average crystal size (integral breadth) of the reflections. Lattice parameters and crystallite size of all phases were refined. Structural data for the known phases were taken from PDF-2 database with PDF numbers: anatase [21-1272], rutile [21-1276], and brookite [29-1360].

Raman spectroscopy was carried out with a Bruker Optics IFS66v/s FTIR spectrometer with FRA-106 Raman attachment. For each spectrum, 32 scans of the undiluted sample in backscattering geometry were measured.

(26) Ohtani, B. *Chem. Lett.* **2008**, *37*, 216–229.

Field emission-scanning electron microscope (FE-SEM) measurements were carried out on a JEOL JSM-6700F field-emission instrument using a secondary electron detector (SE) at an accelerating voltage of 2 kV. High-resolution transmission electron microscopy (HRTEM) was performed at 200 kV on a field-emission instrument of the type JEM-2100F (JEOL Ltd., Tokyo, Japan) with an ultrahigh resolution pole piece (CS = 0.5 mm, CS = 1.2 mm), which provides a point-resolution better than 0.19 nm. Sample preparation was made by dispersing powder in ethanol and dropping ca. 10 μL of the suspension onto a copper-supported perforated carbon film of the type Multi A (Quantifoil Micro Tools GmbH, Jena, Germany), on which it was dried. Observation of powder particles was made in specimen areas, which were locally not supported by the carbon film.

Single-point standard BET surface area measurements were carried out employing a Micromeritics AutoMate 23 instrument. The gas mixture used for the adsorption determinations was 30% nitrogen and 70% helium. The TiO_2 samples were previously heated to 150 °C for approximately 60 min in order to clean the surface of adsorbed organic compounds and humidity.

Photocatalytic Molecular Hydrogen Production. The photocatalytic molecular hydrogen production tests have been performed in a double jacket Duran glass reactor (110 cm^3) with three outlets as described elsewhere.[27] The inner part of the reactor is a cylindrical tube with a diameter of 4 cm and a height of 6.0 cm. In a typical run, 0.0375 g of the Pt loaded TiO_2 photocatalyst has been suspended in 75 mL of an aqueous methanol solution (4.93 mol L^{-1}) by sonication. The suspension was transferred to the photoreactor and bubbled with Ar for 30 min to remove any dissolved O_2. The reactor was sealed with a silicone rubber septum and repeatedly flushed with Ar for another 30 min until no O_2 and N_2 were detected by gas chromatography in the headspace above the solution. Subsequently, the stopcocks were closed and the photoreactor was connected to the cooling system. The photoreactor was irradiated from the outside using a Osram XBO 1000 W xenon lamp in a Müller LAX 1000 lamp housing. The evolved gas was sampled at a constant rate through the silicone rubber septum using a locking-type syringe. The sampled gas was quantitatively analyzed using a gas chromatograph (Shimadzu 8A, TCD detector). The GC was equipped with a molecular sieve 5 A packed column for hydrogen analysis. Ar was used as the carrier gas.

The incident photon flux in the wavelength range 300 nm $\leq \lambda \leq$ 400 nm was determined by ferrioxalate actinometry[12] to be 3.62×10^{-7} Einstein s^{-1}. The lamp was switched on 30 min before the beginning of the reaction to stabilize the power of its emission spectrum. The actinometry was performed in the same photochemical reactor with the same volume of actinometric solution as the photocatalytic test, eliminating the errors associated with the influence of light reflections and reactor geometry. A water bath and a black cutoff filter (3 mm, UG1 SCHOTT glass) were used during photon flux and photonic efficiency measurements.

Flatband Potential Measurements. The flatband potentials have been measured by impedance spectroscopy using Mott–Schottky plots. TiO_2 nanomaterial paste for the fabrication of electrodes for impedance measurements was obtained by mixing 1 mL of water and 100 mg of TiO_2 nanomaterial powder homogeneously by sonication. An appropriate amount of the TiO_2 suspension was spread on a conductive fluorine–tin oxide (FTO) glass with a glass rod, using adhesive tapes as spacers followed by drying in air at 100 °C for 2 h. The electrical contact was formed on the uncoated area of the substrate using silver paint and copper wire. This contact area was later covered with nonconducting epoxy resin to isolate it from the electrolyte solution. A glass rod was placed over the copper wire for better handling. The electrochemical setup for impedance measurements consisted of three electrodes: the working electrode (TiO_2 film), a platinum wire used as counter electrode, and Ag/AgCl, NaCl (3.0 M) electrode as reference (+0.21 vs NHE). The experiments were performed in aqueous 0.1 M KCl solutions at pH 7. The potential was systematically varied between +1.00 and −1.00 V with the frequency range being modulated between 10 and 1000 Hz by an IVIUMSTAT electrochemical interface and impedance analyzer.

Quasi-Fermi Level Measurements. The quasi-Fermi energy was measured according to the method of Roy et al. using methylviologen dichloride (MV^{2+}, E_{red} = −0.44 V) as a pH independent redox system.[21] In a typical experiment, 30 mg of the photocatalyst and 6 mg of methylviologen dichloride were suspended in a 100 mL flask in 50 mL of 0.1 M KNO_3. A platinum flag and Ag/AgCl served as working and reference electrodes, respectively, and a pH meter for recording the proton concentration. HNO_3 (0.1 M) and NaOH (0.1 M) were used to adjust the pH value. The suspension was magnetically stirred and purged with nitrogen gas throughout the experiment. Initially, the pH of the suspension was adjusted to around pH 1. Then, the suspension was irradiated by an Osram XBO 450 W xenon lamp in a Müller LAX 1000 lamp housing. Stable photovoltages between the working and reference electrodes were recorded about 30 min after changing the pH value by a VOLTCRAFT digital multimeter.

Band Gap Energy Measurements. A Varian Cary 100 Scan UV–visible system equipped with a labsphere diffuse reflectance accessory was used to obtain the reflectance spectra (Kubelka–Munk function, F(R)) of anatase and brookite powders over a range of 200–800 nm. Labsphere USRS-99–010 was employed as a reflectance standard.

Photocatalytic Dichloroacetic Acid (DCA) Degradation. The photocatalytic DCA degradation has been measured in a 60 mL double jacket quartz glass reactor. In a typical run, 0.03 g of the photocatalyst was suspended in 60 mL of aqueous10 mM KNO_3 by sonication before the additions of DCA into the slurry (initial DCA concentration 1 mmol L^{-1}). The pH was then adjusted to pH 3 by addition of 0.1 M HNO_3 or NaOH as needed. The temperature of the suspension was maintained at 25 °C. The suspension was vigorously stirred without illumination for 30 min to attain adsorption equilibrium of the DCA molecules on the photocatalyst surface and continuously purged with air to ensure a constant O_2 concentration throughout the experiment. After this adsorption period, UV illumination was provided by a high-pressure Xe-lamp (OSRAM HBO 450 W). A UV(A)/Vis illumination was achieved employing a band-pass filter (WG 320) which eliminates UV-radiation below λ = 320 nm. The intensity of UV(A) illumination was 60 mW/cm^2 at the entrance window of the photoreactor as measured by a UV light meter (ultraviolet radiometer LTLutron UVA-365).

The photocatalytic degradation of dichloroacetic acid was performed at pH 3. The pK_a of DCA is 1.29,[28] and it, thus, exists in its anionic form in aqueous solutions at pH > 2. The

(27) Kandiel, T. A.; Dillert, R.; Bahnemann, D. W. *Photochem. Photobiol. Sci.* **2009**, *8*, 683–690.

(28) Lide, D. R. In *Handbook of Chemistry and Physics*, 70th ed.; CRC Press: Boca Raton, FL, 1990.

photocatalytic oxidation of one DCA anion results in the formation of one proton, two CO_2 molecules, and two Cl^- ions according to eq 3. The pH of the suspension was maintained constant during the photocatalytic experiments using a pH-stat technique as described by Bahnemann et al.[25]

$$CHCl_2COO^- + O_2 \xrightarrow{h\nu,TiO_2} 2CO_2 + H^+ + 2Cl^- \quad (3)$$

The rate of the photodegradation of DCA was followed by measuring the amount of OH^- added to keep the pH constant, thus measuring the amount of H^+ formed which is equivalent to the amount of DCA degraded. The mineralization of DCA was confirmed by TOC measurements at the end of the experimental runs. In all runs, more than 90% DCA removal was observed. The photonic efficiencies (ζ) of the photocatalytic degradation of DCA were calculated as the ratio of the initial degradation rate of DCA and the incident photon flux according to eqs 4 and 5, where the initial degradation rate is calculated from the slope of the individual concentration versus time profiles (see Figure 11). The incident photon flux per volumetric unit has been calculated to be 3.31×10^{-2} Einstein L^{-1} h^{-1} based upon the UV-A light meter measurements and assuming an average illumination wavelength λ = 350 nm; the irradiated surface area was 3.14 cm^2, and the volume of the suspension was 0.06 L.

$$I_0 = \frac{I\lambda}{N_A hc} \quad (4)$$

$$\zeta\,(\%) = \frac{kc_0V}{I_0A} \times 100 \quad (5)$$

with I_0 being the photon flux, I the light intensity, N_A Avogadro's number, h the Planck constant, c the light velocity, k the initial rate constant, A the illuminated area, c_0 the initial DCA concentration, λ the illumination wavelength, and V the reactor volume.

Acknowledgment. T.A.K. thanks the Egyptian Ministry of Higher Education for providing him a doctoral scholarship.